Cancer Nano (2011) 2:95–103
DOI 10.1007/s12645-011-0019-3

ORIGINAL PAPER

Enhanced photodynamic efficacy and efficient delivery of Rose Bengal using nanostructured poly(amidoamine) dendrimers: potential application in photodynamic therapy of cancer

Krishnamoorthy Karthikeyan · Anish Babu · Sang-Jae Kim · Ramachandran Murugesan · Kadarkaraithangam Jeyasubramanian

Received: 28 June 2011 / Accepted: 27 July 2011 / Published online: 13 August 2011

Abstract Photodynamic therapy (PDT) is a promising treatment methodology whereby diseased cells and tissues are destroyed by reactive oxygen species (ROS) by using a combination of light and photosensitizers (PS). The medical application of Rose Bengal (RB), photosensitizer with very good ROS generation capability, is limited due to its intrinsic toxicity and insufficient lipophilicity. In this report, we evaluate the potential of polyamidoamine (PAMAM) dendrimers in delivering RB and its phototoxic efficiency towards a model cancer cell line. The spherical, nanoscaled dendrimers could efficiently encapsulate RB and showed characteristic spectral responses. The controlled release property of dendrimer–RB formulation was clearly evident from the in vitro drug release study. ROS generation was confirmed in dendrimer–RB system upon white light illumination. Photosensitization of Dalton's Lymphoma Ascite (DLA) cells incubated with dendrimer–RB formulation caused remarkable photocytotoxicity. Importantly, the use of dendrimer-based delivery system reduced the dark toxicity of RB.

Keywords Photodynamic therapy · Dendrimer · Drug delivery · Phototoxicity · Dark toxicity · Reactive oxygen species

1 Introduction

Photodynamic therapy is a method of clinical treatment whereby diseased cells and tissues are destroyed by a combination of light and special drugs called photosensitizers (Lopez et al. 2010; Silva et al. 2009; Roy et al. 2003). In addition, the presence of adequate molecular oxygen in the tissue is also required. These components, tolerated singly by the diseased cells, generate cytotoxic oxygen-based molecular species when combined in proper dosage and concentration (Robertson et al. 2009; Guo et al. 2010). PDT is noninvasive and is recognized as a useful initial treatment for malignant tumors (Dolmans et al. 2003; Macdonald and Dougherty 2001). PDT using porfimer sodium (Photofrin®) has been approved for the treatment of esophageal cancer in the United States and Canada, early

Electronic supplementary material The online version of this article (doi:10.1007/s12645-011-0019-3) contains supplementary material, which is available to authorized users.

K. Karthikeyan · S.-J. Kim
Nanomaterials and System Laboratory,
Department of Mechanical Engineering, Jeju National University,
Jeju, South Korea

K. Karthikeyan (✉) · K. Jeyasubramanian (✉)
Department of Nanoscience and Technology,
Mepco Schlenk Engineering College,
Sivakasi, Tamilnadu, India
e-mail: karthi.nanotech@gmail.com
e-mail: kjeyasubramanian@yahoo.co.in

A. Babu · R. Murugesan
School of Biological Sciences, Madurai Kamaraj University,
Madurai, Tamilnadu, India

and late stage lung cancers in the Netherlands, bladder cancer in Canada, and early stage lung, esophageal, gastric and cervical cancers in Japan (Fisher et al. 1996). Photosensitizers can be divided into hydrophilic and hydrophobic compounds. The major drawbacks of the hydrophobic photosensitizers are that they cannot be simply injected intravenously since they form aggregates in solution that restricts their medical applications (Orenstein et al. 1996; Labouebe et al. 2006). Hence, hydrophobic photosensitizers need complex formulation for systematic delivery (Fenga et al. 2004; Shive and Anderson 1997). Hydrophilic photosensitizers are advantageous than hydrophobic photosensitizers since they can be easily delivered intravenously and significantly improve tumor killing (Moore et al. 2009; Vrouenraets et al. 2002). However, hydrophilic photosensitizers poorly accumulate in tumor cells as it finds difficulty in crossing cell membranes. This is mainly because the cellular transport systems in cancer cells are slowly accelerated for hydrophilic drugs to pass through when compared to normal cells (Kessel 1981).

Rose Bengal (RB) is a hydrophilic photosensitizer with a high absorption coefficient in the visible region of the spectrum at 552 nm showing good quantum yield of singlet oxygen (Kochevar et al. 1996). Although it has potential in photodynamic therapy of tumors, its tendency to aggregate in solution under physiological condition decreases the yield of reactive oxygen species (ROS) (Killig et al. 2004). Therefore, it is essential to have an appropriate formulation for the delivery of this hydrophilic photosensitizer in therapeutic levels. The ideal drug delivery system for carrying PDT should be biodegradable, have minimum toxicity, incorporate the photosensitizer without loss or alteration of the sensitizer activity and provide an environment where the photosensitizer can be administered in monomeric form (Konan et al. 2002). Importantly, the delivery system should enable selective accumulation of the PS within the diseased tissue in therapeutic concentrations with little or no uptake by nontarget cells (Chatterjee et al. 2008).

It is expected that charged or slightly lipophilic nanoscaled drug delivery systems can be used for efficient delivery of highly hydrophilic photosensitizers for PDT of cancer. In this regard, the use of dendrimer-based nanocarriers is a promising method for the tumor specific delivery of PS. Nanoparticles, such as nanospheres and nanocapsules, possess high impact in delivery system as PS carriers because they can meet all the requirements for an ideal PDT agent (Premanathan et al. 2011; Murday et al. 2009; Koo et al. 2005). Dendrimers can be considered as the most versatile, compositionally and structurally controlled synthetic nanoscale building blocks available today (Koda et al. 2008; Bechet et al. 2008). Dendrimers have high degree of molecular uniformity, loading capacity, biocompatibility and a highly functionalized terminal surface that facilitates modification of the solubility of drugs to help target the drug to its therapeutic sites, or to alter the release profile of the therapeutic agent (Svenson and Tomalia 2005; Jansen et al. 1994). With the aim of improving the drug delivery and release kinetics suitable for carrying PDT and diminishing the dark toxicity of RB, dendrimer-based delivery system could be a better choice.

The present study relies on polyamidoamine (PAMAM) dendritic nanostructures as an efficient drug delivery system for a well-known hydrophilic photosensitizer, Rose Bengal that was evaluated by investigating the interaction between the dendrimer and RB and the photodynamic efficacy. However, our studies explored the influence of G2.5 PAMAM+RB on Dalton's Lymphoma Ascite (DLA) cancer cell lines. A potential application of PAMAM dendrimers as an efficient drug delivery system for a hydrophilic photosensitizer will provide new opportunities in nanomedicine for PDT of cancer.

2 Material and methods

2.1 Materials

Methanol was obtained from Spectrum Chemicals, India. Methyl acrylate was procured from Loba Chemicals, India. Ethylenediamine, ammonium molybdate, pyridine and diethyl ether were obtained from Merck, India. Ammonia and potassium iodide were obtained from SD Fine Chemicals, India. Rose Bengal was purchased from Aldrich, USA. Dialysis tubing (12–14 kDa cutoff size) was obtained from Himedia, India. All the chemicals were used as received except methanol, which was distilled twice before use.

2.2 Synthesis of PAMAM dendrimer

PAMAM dendrimers with various generations have been synthesized using a divergent method. The synthesis of PAMAM dendrimers undergoes Michael addition reaction (Hedden and Bauer 2003). Ammonia and 100 equiv. of methylacrylate (MA) were dissolved in methanol, respectively. Ammonia solution was added to MA solution dropwise. Reaction mixture was stirred in 37°C for 2 days. After reaction, solvent was removed by a rotary evaporator and residual product was stored in vacuum.

$$NH_3 + 3CH_2CHCOOCH_3 \xrightarrow{37^{\circ}C \text{ for } 48 \text{ hrs}} N(CH_2CH_2COOCH_3)_3 \quad (G0.5)$$

PAMAM G 0.5 and 100 equiv. of ethylenediamine (EDA) was dissolved in methanol, respectively. PAMAM

solution was added to EDA solution and stirred at 50°C for 2 days. After reaction was completed, solvent was removed using a rotary evaporator. Residual product was precipitated in ethyl ether two times and stored in vacuum.

$$\mathrm{N(CH_2CH_2COOCH_3)} + 3\mathrm{NH_2CH_2NH_2} \xrightarrow{50^\circ\mathrm{C}\,48\,\mathrm{hrs}} \mathrm{N(CH_2CH_2CONHCH_2CH_2NH_2)_3} + 3\mathrm{CH_3OH} \quad \text{(G1.0)}$$

The first generation dendrimer G1.0 was purified by three times centrifugation and redispersion in methanol. Addition of MA in proper molar ratios with G1.0 under heating (50°C) for 48 h results in production of G1.5 PAMAM dendrimer. Subsequent addition of EDA generates G2.0 dendrimer. Likewise, the chain reaction is continued till the synthesis for G2.5 dendrimer. The dendrimer was purified at each step by centrifugation for 30 min at 16,000*g* and resuspending in methanol solution. Finally, the dendrimer solution was dialyzed against methanol water (1:10) mixture for 24 h in order to remove any nonreacted chemical species.

2.3 Encapsulation of Rose Bengal into the PAMAM dendritic box

The G2.5 PAMAM dendrimer and RB were mixed in the ratio of 10:1 in a solution of 20 ml of methanol and 5 ml of water. The resulting solution was vigorously stirred at 500 rpm for 24 h using a magnetic stirrer. After 24 h, the solvent was removed under vacuum using a rotary evaporator. The final product obtained was purified by centrifugation at 16,000*g* for 30 min followed by dialysis and stored at 4°C.

2.4 Characterization techniques

Surface morphology of G2.5 PAMAM dendrimer was analyzed using atomic force microscopy (AFM) in contact mode using XE 70, SPM, Park System, South Korea, in a scan area of 20 μm. The sample preparation was performed by taking 5 μl of G2.5 PAMAM and diluting 100 times. The zeta potential analysis was performed at 25°C, in MilliQ® water using Zetasizer Nano, Malvern Instruments, UK. A few drops of the prepared solution were allowed to spin coat on a glass substrate for 10 min and then dried before measurement. UV–vis spectra (Lambda 25, Perkin Elmer, USA) of PAMAM dendrimers were measured in methanol:water (50% *v/v*). Fourier transform infrared (FTIR) spectra of the samples were recorded in liquid mode using a modern Bruker optic GmbH-Alpha T spectrometer, Germany. Fluorescence spectra of were obtained in aqueous environment using a spectro-flourimeter (Jasco FP-6300, Japan).

2.5 Estimation of drug loading and encapsulation efficiency

The amount of drug loaded into the dendrimer and the encapsulation efficiency of the G2.5 PAMAM dendrimers were measured spectrophotometrically, using the formulas given below:

$$\text{Drug loading}\,(\%) = [\mathrm{W_1}/\mathrm{W_2}] \times 100 \quad (1)$$

$$\text{Encapsulation efficiency} = [(\mathrm{W_3} - \mathrm{W_4})/\mathrm{W_4}] \times 100 \quad (2)$$

where

W_1 weight of the drug present in dendrimer
W_2 net weight of the dendrimer
W_3 weight of the drug added, and
W_4 weight of the drug released into the supernatant.

2.6 Measurement of drug release kinetics

The release of RB from the G2.5 PAMAM was measured spectrophotometrically as follows: 50 mg of RB encapsulated dendrimer was made up to 1 ml using a mixture of methanol: water (50:50, v/v). This solution was dialyzed using a dialysis tubing with a MW cutoff 12,000–14,000 Da (~2.4 nm) (Himedia, India) against phosphate buffer saline (PBS) of pH 7.4 at 37°C with mild stirring. This was continued for 72 h and at each time interval 1 ml was withdrawn from the PBS for spectrophotometric analysis at λ_{max} 540 nm and was replaced by fresh PBS of the same amount. A graph was plotted with cumulative release% against time interval in hours representing the drug release profile.

2.7 Light source for PDT

A 150 W xenon arc lamp was used as a light source. The therapeutic window was adjusted by using 10% KI (5 cm path length) and pyridine (1 cm path length) as a filter for UV radiation. The specimen was kept in an open quartz cuvette and air saturated by magnetic stirring. It was irradiated at a distance of 12 cm from the light source.

2.8 Measurement of quantum yield of ROS generation by iodide method

The iodide assay was used for the evaluation of ROS generation of RB encapsulated G2.5 PAMAM dendrimers (Mosinger and Micka 1997). This assay is based on the reaction of singlet oxygen ($^1O_2$) (produced in the photodynamic reaction) with I^- in the presence of ammonium

molybdate as a catalyst. The reaction product is I_3^-, the amount of which (measured spectrophotometrically at λ= 351 nm) is directly proportional to the generated $^1O_2$.

2.9 *In vitro* cell viability test—MTT assay

For MTT cell viability assay, 2.5×10^4 DLA cells per well were seeded onto a well of 96-well plates in RPMI 1640 media for 2 h incubation, treated with various concentrations of RB in free and dendrimer encapsulated form and photoirradiated for 10 min using a xenon arc lamp. The media was changed to fresh RPMI 1640 media with 10% PBS and incubated for 12 h. Then, 5 mg/ml MTT solution (20 µl/well) was added to each well, and cells were incubated for an additional 4 h at 37°C. The supernatant was aspirated and 100 µl of isopropanol was added to the wells to dissolve any blue precipitate present. The absorbance was then measured at 570 nm by a microplate reader. Cell viability was calculated using the following formula:

$$\text{Cell viability} = (\text{Average absorbance of treated group}/\text{Average absorbance of the control group}) \times 100 \quad (3)$$

3 Results and discussion

3.1 Synthesis and characterization of PAMAM dendrimers

The PAMAM dendrimers of various generations (G0.5, G1.0, G1.5, G2.0 and G2.5) are synthesized using the Michael addition method as described in the previous section. The PAMAM dendrimers with ammonia as the core molecule possess an ester group (R-COO-R) and amine (R-CO-NH_2) group as terminal surfaces in the successive half and full generation. The various generation dendrimers were characterized by UV–vis spectroscopy, FTIR spectroscopy, AFM and zeta potential. The UV–vis spectroscopy of all generations of PAMAM dendrimers shows a characteristic absorption at 275 to 290 nm (Figure S1). The FTIR spectra of the half generation (G0.5/G1.5/G2.5) shows a characteristic –C=O stretching vibrations around 1,729 cm^{-1} due to the presence of a free ester (C=O) group in the end surface (Kolhe et al. 2003). In addition to this, a band at 1,000 cm^{-1} to 1,200 cm^{-1} also appeared, which is assigned to the –C–O stretching mode [Fig. 3, 2.5 PAMAM]. The FTIR spectrum of the full generation dendrimers shows characteristic N–H stretching vibrations around 1,620–1,650 cm^{-1} because of the reaction of ester with amine making it as an amine end (Figure S2).

From the zeta potential values of various generations, it is possible to evaluate the nature of the surface groups present in the dendrimers (Tomalia et al. 2007). The half generation PAMAM dendrimers are electrically neutral and show positive potential values. The full generation PAMAM dendrimers are electronegative and they possess negative potential values. The zeta potential data also confirmed the presence of the charged/neutral terminals at the surfaces. The zeta potential values of all the PAMAM dendrimers of various generations are given in Table 1. The AFM images of the 2.5 G PAMAM dendrimer (2D and 3D) recorded in noncontact mode is given as Fig. 1(a) and (b) respectively. From the image, it is clear that most of the

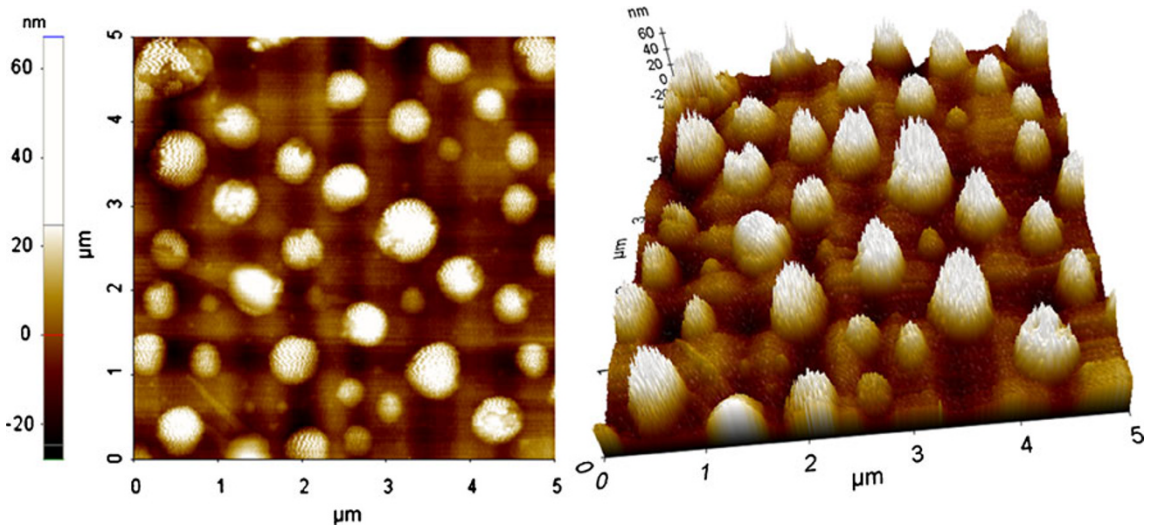

Fig. 1 Surface morphology of G2.5 PAMAM dendrimer measured using AFM

particles appeared spherical in shape with particle size around 20 nm.

3.2 Dendrimer–Rose Bengal interaction

The dendritic cavity present in the dendrimer molecules enables them to hold the guest molecule (drug). Such host–guest interactions can be successfully followed spectrophotometrically. UV–visible absorption peak of G2.5 dendrimer and the RB drug in methanol is shown as in Fig. 2. The dendrimer shows an absorption band in the UV region around 270–280 nm and the free RB shows a peak at 552 nm (Fig. 2) (Fini et al. 2007). A weak band appearing around 500 nm is a measure of aggregation of the RB molecules in solution (Xu and Neckers 1989). On mixing equimolar amounts of dendrimer and the drug, the band appearing in the visible region (around 552 nm) is shifted towards 545 nm. Because of the movement of drug molecules into the dendritic entity, noncovalent interactions between the RB and the internal cavities of PAMAM dendrimers make such a blue shift (Cheng et al. 2007). In addition to this, intermolecular interaction between the carboxyl group of RB and the terminal groups of PAMAM dendrimers also makes such blue shift (Gigimol and Mathew 2007). In the UV–vis spectra of the G2.5 PAMAM+RB, there is no observation of broad shoulder peak around 500 nm since on encapsulation, the delocalization of the lone pair of electrons present in the RB molecule with dendrimer (Finia et al. 2004). These results concluded that the RB molecules interact well with G2.5 PAMAM dendrimers through cavity encapsulation.

FTIR spectroscopy is also used to study the host–guest interactions. The FTIR spectra of G2.5 PAMAM dendrimer, free RB and the G2.5 PAMAM+RB are shown in Fig. 3. The FTIR of G2.5 PAMAM dendrimer shows characteristic

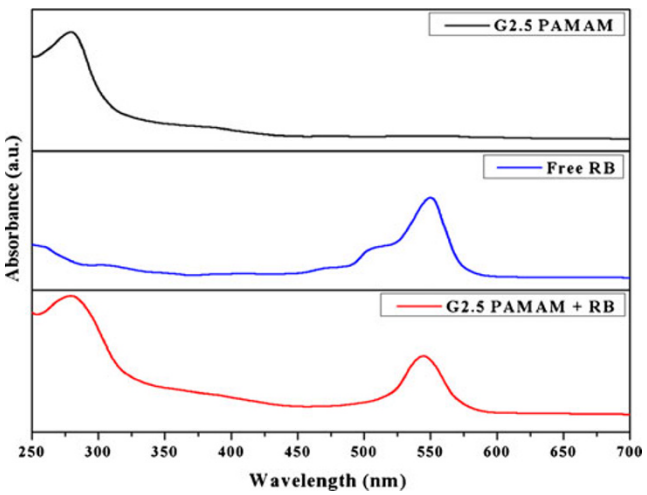

Fig. 2 UV–vis spectra of G2.5 PAMAM dendrimer, free RB and G2.5 PAMAM+RB

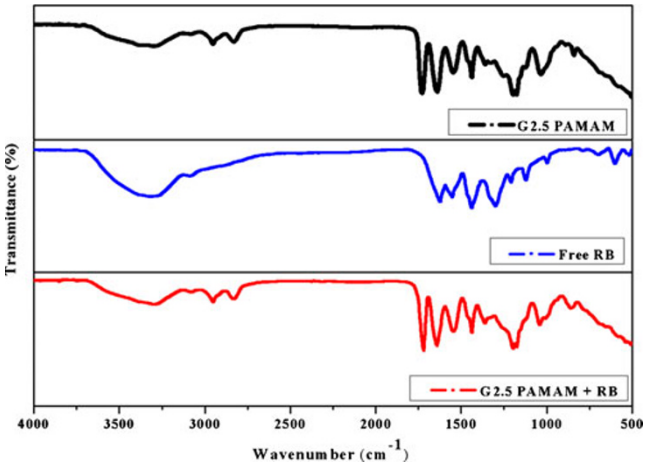

Fig. 3 FTIR spectra of G2.5 PAMAM dendrimer, free RB and G2.5 PAMAM+RB

C=O stretching vibrations around 1,729 cm^{-1} that is assigned to an ester group (present as free terminal group in G2.5 dendrimer). The band at 1,641 cm^{-1} is assigned to N–H deformation vibration present in the amide group (Kolhe et al. 2003). In addition to this, a 1,000 cm^{-1} to 1,200 cm^{-1} band is assigned to the C–O stretching mode. Peaks in the region 2,800–3,200 cm^{-1} corresponds to N–H stretching and C–H stretching vibrations (Devarakonda et al. 2007). The FTIR spectra of RB shows a characteristic C=O stretching at 1,620 cm^{-1} (Jhonsi et al. 2009). All the bands were found individually on the dendrimer and the drug shifts if both are mixed together. The C=O and N–H deformation bands shifted to lower frequencies 1,718 cm^{-1} and 1,540 cm^{-1} that could be explained by intermolecular hydrogen bonding between electronegative atoms in the RB with the G2.5 PAMAM dendrimer. These observations reveal that the RB molecules are encapsulated in the dendritic box through their carboxyl group via electrostatic interaction.

Further, the interaction between RB and PAMAM dendrimer was also studied by fluorescence quenching measurements. Figure 4 represents the effect of PAMAM dendrimer on the fluorescence spectra of RB. The G2.5 PAMAM+RB showed decreased emission intensity, compared to free RB. Further, there is no band shift in the spectra of dendrimer–RB complex compared to free RB, indicating that no structural change occurred. The quenching observed is due to the electronegative carboxyl group of RB, which increased the interaction of dye with the dendrimer (Jhonsi et al. 2009). Zeta potential measurements enable the understanding of the interaction of RB and dendrimer moieties. G2.5 PAMAM dendrimer possesses a surface charge of +0.168 mV. Upon interaction with RB the surface charge of the dendrimer changed to −1.33 mV. This may be due to the presence of surface attached RB molecules that are having more electronegative chlorine

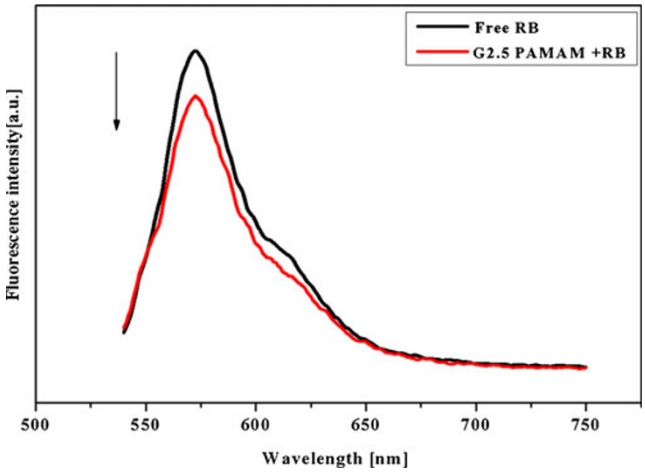

Fig. 4 Fluorescence spectra of free RB and G2.5 PAMAM+RB

atoms and a keto group in the molecule. Hence, the above characterization techniques reveal that the RB molecules are encapsulated in the dendritic cavity and also some of the RB molecules are absorbed at the terminal surface of the PAMAM dendrimers.

3.3 Drug loading and encapsulation efficiency of G2.5 PAMAM+RB nanocapsules

High drug loading and better encapsulation efficiency is expected for an ideal drug delivery agent, thereby, reducing the quantity of the matrix materials for drug administration (Mohanraj and Chen 2006). The drug loading in the G2.5 PAMAM+RB is through the absorption technique. Hence, the delivery system should be ideal in case of drug loading efficiency and drug release kinetics for carrying PDT, not suppressing the quantum yield of the PS after encapsulation. The amount of drug loaded into the dendrimer and the encapsulation efficiency of the G2.5 PAMAM dendrimers were measured spectrophotometrically during purification of G2.5 PAMAM+RB by centrifugation and are to be observed as 1.8% and 92.5% respectively.

3.4 *In vitro* drug release kinetics of G2.5 PAMAM+RB

In our G2.5 PAMAM+RB, the RB molecules are physically encapsulated in the cavity of the PAMAM dendrimer and a minimum quantity is absorbed at the terminal surface. The possible drug release kinetics is through diffusion process (Kedar et al. 2010). Figure 5 shows the in vitro drug release profile of the RB encapsulated G2.5 PAMAM dendrimers followed spectrophotometrically for a period of 72 h. It is observed that the systematic release of RB after 12, 24 and 48 h are 35%, 50% and 74% respectively. After 72 h, 83% of drug release is noticed. From the graph, it is clear that the rate of release of RB from the dendrimer at the initial stage

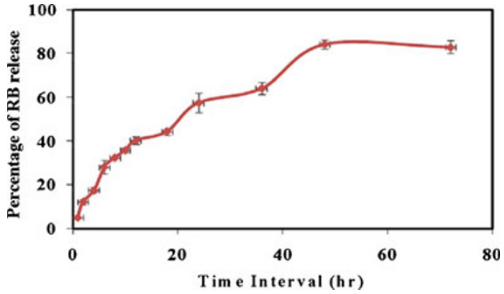

Fig. 5 RB release kinetics from the G2.5 PAMAM+RB

is high whereas on the final stage it is found as low. The quicker release in the initial hours is the release of small amount of RB attached to the surface groups of the dendrimer. The drug release becomes somewhat slower, i.e., after 12 h is probably due to the encapsulated drug that is present in the dendritic cavity or the inner core of PAMAM. Sustained release was noticed after 48 h. The drug release studies shows that G2.5 PAMAM dendritic system possesses excellent controlled release properties suitable for carrying PDT of hydrophilic photosensitizers.

3.5 ROS quantum efficiency of G2.5 PAMAM+RB

The significant factor influencing the PDT efficiency is the quantum yield of ROS generation from the PS. The ROS generation of free RB and its encapsulated form was evaluated by determining the quantum yield by iodide method. It is experimentally found that the $^1O_2$ quantum yield for free RB is 0.76. The $^1O_2$ quantum yield for G2.5 PAMAM+RB was measured as 0.71 from using the iodide method (Mosinger and Micka 1997). Figure 6 depicts the graphical representation of the change in absorbance of the iodide band (351 nm) against the irradiation time for variously concentrated solutions of RB encapsulated in G2.5 PAMAM dendrimers. It is clear from Fig. 6. that the

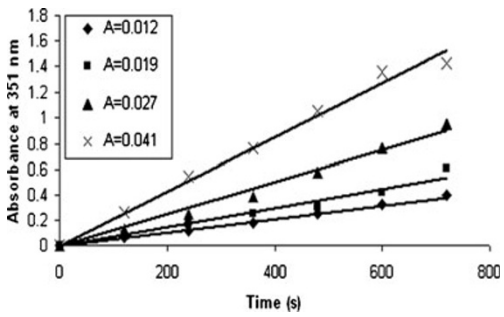

Fig. 6 Estimation of quantum yield of ROS generation from the nanocapsules by the iodide method. *Graph* shows the change in absorbance of the iodide band (351 nm) against the irradiation time for variously concentrated solutions of RB encapsulated in G2.5 PAMAM dendrimers

absorption of the iodide band increases with the increase in the concentration of the G2.5 PAMAM+RB, which indirectly show the increase in the ROS generation of G2.5 PAMAM+RB at higher concentration. These results strongly demonstrate that the G2.5 PAMAM can be an ideal drug delivery agent since no such alteration in the ROS activity is noticed when compared to the activity of the free RB.

3.6 Phototoxicity and dark toxicity of G2.5 PAMAM+RB

The aim was to investigate the photosensitizing activity of G2.5 PAMAM+RB against DLA cells and its efficiency as a potential PDT treatment for cancer. The cell viability of DLA cells upon photoirradiation as a function of concentration of G2.5 PAMAM+RB indicates the photodynamic effect in vitro. Figure 7 illustrates the photodynamic effect on the DLA cell line, as a function of the photosensitizer concentration. The free RB produced the lower photodynamic effect when compared to G2.5PAMAM+RB. The beneficial effect of the RB loaded dendrimers was mainly highlighted at a RB concentration of 510 nM. When the doses of the free RB and the G2.5 PAMAM+RB are increased to 510 nM, it was found that the cell viability percentage for G2.5 PAMAM+RB-treated cells was 24.9% when compared to the 38% cell viability for free RB-treated cells. The phototoxicity results show that the G2.5 PAMAM+RB are more toxic to the DLA cells compared to the toxicity of free RB. PAMAM dendrimer is a hyperbranched molecule and the amount of drug loading is as low as 1.8%, which ensures the uniform distribution of the photosensitizer in the dendritic matrix and this enables sustained drug release kinetics suitable for carrying PDT.

Low dark toxicity is one of the significant criteria for assessing the usefulness of photosensitizers, since the major side effects in clinical PDT result from the dark toxicity of photosensitizer to normal tissue. From Fig. 8, at lower concentration of the free RB, the cell viability is 92% and

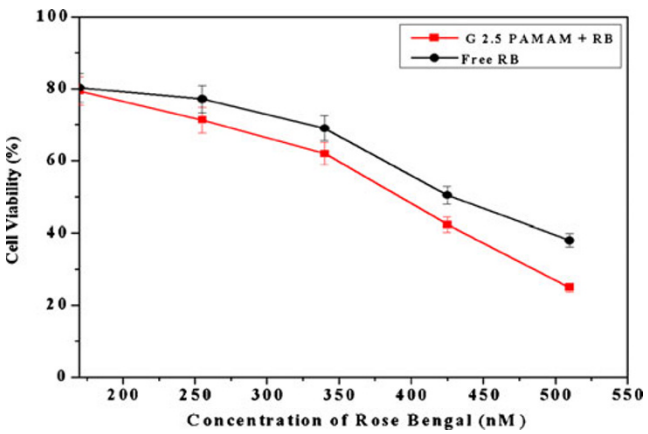

Fig. 7 Phototoxicity of free RB and G2.5 PAMAM+RB

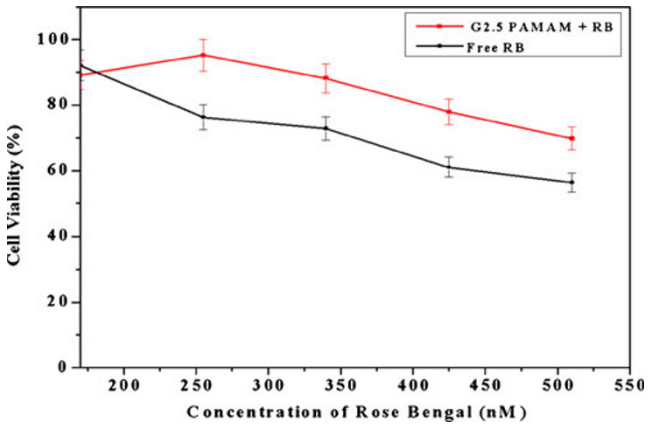

Fig. 8 Dark toxicity of free RB and G2.5 PAMAM+RB

an increase in concentration of the free RB to 510 nM makes it more toxic and the cell viability is reduced to 56%. The dark toxicity of the RB-loaded dendritic nanostructures exhibits nontoxic at lower concentrations and is less toxic at higher concentrations (the cell viability is 69.8% at 510 nM) as compared to the dark toxicity of free RB. The very low toxicity of G2.5 PAMAM+RB might result from the good biocompatibility and low toxicity of PAMAM dendrimers (Koda et al. 2008; Bechet et al. 2008; Svenson and Tomalia 2005). It can be highlighted that differential toxicity was observed for G2.5 PAMAM+RB in the presence and absence of light against cancer cells. Therefore, the efficient photodynamic efficacy of G2.5 PAMAM+RB, together with the above-mentioned advantages, makes this type of formulation for delivery of photosensitizer in PDT potentially very useful for clinical application.

4 Conclusion

PAMAM dendritic nanostructures could effectively deliver RB photosensitizers into cancer cells and produce enhanced photodynamic efficacy. The interaction between the PAMAM dendrimer and RB are investigated by UV–vis and FTIR spectra, fluorescence quenching and zeta potential measurements. Our systemic investigation of the dendrimer-based formulation of RB shows that it is feasible to encapsulate even a hydrophilic photosensitizer with excellent encapsulation efficiency and release kinetics. Results showed that drug release was quite faster in the initial hours and, above 80%, was released in 72 h, which was found to be more satisfactory for a water-soluble photosensitizer. It is observed that the PAMAM dendrimer-based delivery of RB could retain its ROS generation property upon irradiation and also could reduce its toxicity by holding the RB molecules in the internal cavities.

Importantly, the dendritic formulation exhibited minimized dark toxicity within the concentration used and enhanced phototoxicity to DLA cells compared to the dark phototoxicity of free RB. The key findings of our work with the above-mentioned advantages ensure that PAMAM dendrimer-based nanocarriers of PS delivery should be a promising candidate for PDT.

Acknowledgements The authors are thankful to the Management and the Principal of Mepco Schlenk Engineering College for providing the necessary facilities to carry out this work. S.-J. Kim acknowledges support from Korea Research Foundation (KRF) project number 2011–0015829.

References

Bechet D, Couleaud P, Frochot C, Viriot ML, Guillemin F, Heyob MB (2008) Nanoparticles as vehicles for delivery of photodynamic therapy agents. Trends Biotechnol 26:612–621

Chatterjee DK, Fong LS, Zhang Y (2008) Nanoparticles in photodynamic therapy: an emerging paradigm. Adv Drug Deliv Rev 60:1627–1637

Cheng Y, Qu H, Ma M, Xu Z, Xu P, Fang Y, Xu T (2007) Polyamidoamine (PAMAM) dendrimers as biocompatible carriers of quinolone antimicrobials: an in vitro study. Eur J Med Chem 42:1032–1038

Devarakonda B, Otto DP, Judefeind A, Hill RA, Villiers MM (2007) Effect of pH on the solubility and release of furosemide from polyamidoamine (PAMAM) dendrimer complexes. Int J Pharm 345:142–153

Dolmans DEJGJ, Fukumura D, Jain RK (2003) Photodynamic therapy for cancer. Nat Rev Cancer 3:380–387

Fenga SS, Ruanb G, Li QT (2004) Fabrication and characterizations of a novel drug delivery device liposomes-in-microsphere (LIM). Biomaterials 25:5181–5189

Fini P, Loseto R, Catucci L, Cosma P, Agostiano A (2007) Study on the aggregation and electrochemical properties of Rose Bengal in aqueous solution of cyclodextrins. Bioelectrochemistry 70:44–49

Finia P, Longobardi F, Catuccia L, Cosmaa P, Agostiano A (2004) Spectroscopic and electrochemical study of Rose Bengal in aqueous solutions of cyclodextrins. Bioelectrochemistry 63:107–110

Fisher AMR, Mulphree AL, Gomer CJ (1996) Clinical and preclinical photodynamic therapy. Lasers Surg Med 17:2–32

Gigimol MG, Mathew B (2007) Effect of the nature and degree of cross linking on the Rose Bengal uptake by DVB-, NNMBA-, HDODA-, and TTEGDA-cross linked aminopolyacrylamides. J Appl Polym Sci 104:2856–2867

Guo H, Qian H, Idris NM, Zhang Y (2010) Singlet oxygen-induced apoptosis of cancer cells using upconversion fluorescent nanoparticles as a carrier of photosensitizer. Nanomedicine: NBM 6:486–495

Hedden RC, Bauer BJ (2003) Structure and dimensions of PAMAM/PEG dendrimer-star polymers. Macromolecules 36:1829–1835

Jansen JF, Berg EMB, Meijer EW (1994) Encapsulation of guest molecules into a dendritic box. Science 266:1226–1229

Jhonsi MA, Kathiravan A, Renganathan R (2009) Photoinduced interaction between xanthene dyes and colloidal CdS nanoparticles. J Mol Struct 921:279–284

Kedar U, Phutane P, Shidhaye S, Kadam V (2010) Advances in polymeric micelles for drug delivery and tumor targeting. Nanomedicine: NBM 6:714–729

Kessel D (1981) Transport and Binding of Hematoporphyrin derivative and related porphyrins by murine leukemia L1210 cells. Cancer Research 41:1318–1323

Killig F, Stark G, Apell HJ (2004) Photodynamic inactivation of the Na, K-ATPase occurs via different pathways. J Membrane Biol 200:133–144

Kochevar IE, Lambert CR, Lynch MC, Tedesco AC (1996) Comparison of photosensitized plasma membrane damage caused by singlet oxygen and free radicals. Biochimica et Biophysica Acta 1280:223–230

Koda S, Inoue Y, Iwata H (2008) Gene transfection into adherent cells using electroporation on a dendrimer-modified gold electrode. Langmuir 24:13525–13531

Kolhe P, Misra E, Kannan RM, Kannan S, Lai ML (2003) Drug complexation, in vitro release and cellular entry of dendrimers and hyperbranched polymers. Int J Pharm 259:143–160

Konan YN, Gurny R, Allemann E (2002) State of the art in the delivery of photosensitizers for photodynamic therapy. J Photochem Photobiol, B Biol 66:89–106

Koo OM, Rubinstein I, Onyuksel H (2005) Role of nanotechnology in targeted drug delivery and imaging: a concise review. Nanomedicine: NBM 1:193–212

Labouebe MZ, Lange N, Gurny R, Delie F (2006) Hypericin-loaded nanoparticles for the photodynamic treatment of ovarian cancer. Int J Pharm 3:174–181

Lopez T, Ortiz E, Alvarez M, Navarrete J, Odriozola JA, Ortega FM, Mozo EP, Escobar P, Espinoza KA, Rivero IA (2010) Study of the stabilization of zinc phthalocyanine in sol–gel TiO_2 for photodynamic therapy applications. Nanomedicine: NBM 6:777–785

Macdonald IJ, Dougherty TJ (2001) Basic principles of photodynamic therapy. J Porphyrins Phthalocyanines 5:105–129

Mohanraj VJ, Chen Y (2006) Nanoparticles—a review. Trop J Pharm 5:561–573

Moore CM, Pendse D, Emberton M (2009) Photodynamic therapy for prostate cancer—a review of current status and future promise. Nat Clin Prac Urol 6:18–30

Mosinger J, Micka Z (1997) Quantum yields of singlet oxygen of metal complexes of meso-tetralds (sulphonatophenyl) porphine. J Photochem Photobiol, A Chem 107:77–82

Murday JS, Siegel RW, Stein J, Wright JF (2009) Translational nanomedicine: status assessment and opportunities. Nanomedicine: NBM 5:251–273

Orenstein A, Kostenich G, Roitman L, Shechtman Y, Kopolovic Y, Ehrenberg B, Malik Z (1996) A comparative study of tissue distribution and photodynamic therapy selectivity of chlorine6, photofrin II and ALA-induced protoporphyrin IX in a colon carcinoma model. Br J Cancer 73:937–944

Premanathan M, Karthikeyan K, Jeyasubramanian K, Manivannan G (2011) Selective toxicity of ZnO nanoparticles toward Gram positive bacteria and cancer cells by apoptosis through lipid peroxidation. Nanomedicine: NBM 7:184–192

Robertson CA, Evans DH, Abrahamse H (2009) Photodynamic therapy (PDT): a short review on cellular mechanisms and cancer research applications for PDT. J Photochem Photobiol B Biol 96:1–8

Roy I, Ohulchanskyy TY, Pudavar HE, Bergey EJ, Oseroff AR, Morgan J, Dougherty TJ, Prasad PN (2003) Ceramic-based nanoparticles entrapping water-insoluble photosensitizing anticancer drugs: a novel drug-carrier system for photodynamic therapy. J Am Chem Soc 125:7860–7865

Shive MS, Anderson JM (1997) Biodegradation and biocompatibility of PLA and PLGA microspheres. Adv Drug Deliv Rev 28:5–24

Silva AR, Inada NM, Rettori D, Baratti MO, Vercesi AE, Jorge RA (2009) In vitro photodynamic activity of chloro(5,10,15,20-tetraphenylporphyrinato) indium(III) loaded-poly(lactide-co-gly-

colide) nanoparticles in LNCaP prostate tumour cells. J Photochem Photobiol, B Biol 94:101–112

Svenson S, Tomalia DA (2005) Dendrimers in biomedical applications—reflections on the field. Adv Drug Deliv Rev 57:2106–2129

Tomalia DA, Reyna LA, Svenson S (2007) Dendrimers as multipurpose nanodevices for oncology drug delivery and diagnostic imaging. Biochem Soc Trans 35:61–67

Vrouenraets MB, Visser GW, Stigter M, Oppelaar H, Snow GB, Dongen GA (2002) Comparison of aluminium (III) phthalocyanine tetrasulfonate and meta-tetrahydroxyphenylchlorin-monoclonal antibody conjugates for their efficacy in photodynamic therapy *in vitro*. Int J Cancer 98:793–798

Xu D, Neckers DC (1989) Aggregation of Rose Bengal molecules in solution. J Photochem Photobiol, A Chem 47:213–222